CHEMISTRY OF MATERIALS

ARTICLE

pubs.acs.org/cm

Control of the Electronic Properties and Resistive Switching in the New Series of Mott Insulators $GaTa_4Se_{8-y}Te_y$ ($0 \leq y \leq 6.5$)

V. Guiot, E. Janod, B. Corraze, and L. Cario*

Institut des Matériaux Jean Rouxel (IMN), Université de Nantes, CNRS, 2 rue de la Houssinière, BP3229, 44322 Nantes, France

Supporting Information

ABSTRACT: We report here the substitution of Se by Te in the Mott insulator $GaTa_4Se_{8-y}Te_y$, a lacunar spinel compound containing Ta_4 tetrahedral clusters. Our synthetic and crystallographic works show that Te atoms occupy successively two different crystallographic sites and that the substitution reaches a limit for $GaTa_4Se_{1.5}Te_{6.5}$. Band structure calculations and transport measurements demonstrate that this substitution induces for low Te doping ($0 \leq y \leq 4$) an increase of the band gap related to a narrowing of the d bands (i.e., a negative chemical pressure effect). Conversely, for higher Te doping ($y \geq 4$), a decrease of the band gap is observed, while the bandwidth of the d bands stays almost constant. This result suggests that the partial declusterization of Ta_4 tetrahedra observed at high Te doping ($y \geq 4$) leads to a very unusual reduction of the electronic repulsion energy (U) that opens the gap between the lower and upper Hubbard bands. The $GaTa_4Se_{8-y}Te_y$ compounds therefore provide, to our knowledge, the first example of a U-controlled tuning of electronic properties in a Mott insulator. Moreover, we show that the substitution of Se by Te in $GaTa_4Se_{8-y}Te_y$ does not affect drastically the reversible and nonvolatile electric pulse-induced resistive switching phenomena discovered recently in the nonsubstituted compound $GaTa_4Se_8$.

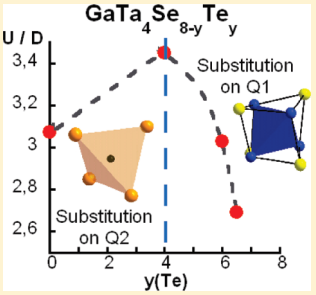

KEYWORDS: lacunar spinel, chalcogenide, Mott insulator, electronic properties, resistive switching

INTRODUCTION

In transition metal compounds with half-filled bands, the presence of strong electronic on-site repulsion (U) often drives the system into a Mott insulator state as the bandwidth (W) is often smaller than U.[1] The proximity to the Mott insulating state depends on the band filling and on the bandwidth W, which can be modified, for example, by electronic doping or external pressure (see Figure 1). Filling-controlled and bandwidth-controlled insulator-to-metal transitions (MIT) were intensively studied during the last decades as transition metal-based Mott insulators often exhibit outstanding properties when they are brought close to the MIT.[1] High-T_c superconductivity in cuprates or colossal magnetoresistance in manganites are examples of such phenomena that may occur at filling-controlled MIT. On the other hand, V_2O_3 or NiS_2 represent archetypal strongly correlated systems that undergo bandwidth-controlled MIT.[1,2] In these systems, external physical pressure increases the bandwidth, which reduces the correlation strength U/W and induces a MIT. Alternatively, the MIT is also achieved in V_2O_3 or NiS_2 by substituting V by Cr, or S by Se, respectively.[1−5] In these systems, it is generally believed that the effects of chemical substitution and physical pressure are qualitatively equivalent,[1,2] and this similarity is often highlighted by the use of the common phrase "chemical pressure effect".

Recently, filling and bandwidth-controlled MITs were investigated in the family of narrow gap Mott insulators AM_4Q_8 (A = Ga, Ge; M = V, Nb, Ta, Mo; Q = S, Se) containing transition-metal tetrahedral M_4 clusters (Figure 2).[6,7] In these compounds, the elementary structural unit on which the Coulomb repulsion U occurs is this M_4 cluster rather than the sole transition metal M. This results in reduced Coulomb repulsion U and Mott−Hubbard gaps (0.1−0.3 eV) as compared to other inorganic Mott insulators.

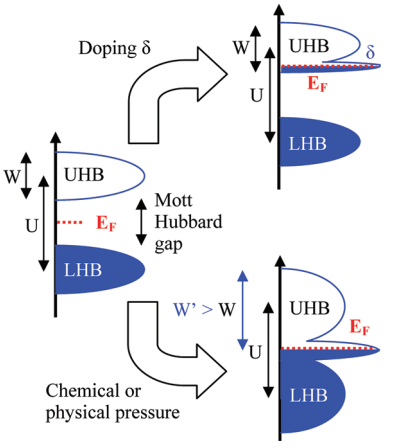

Figure 1. Schematic view of a filling-controlled (δ) and a bandwidth-controlled (W) insulator-to-metal transition (MIT) in a Mott insulator. LHB (UHB) stands for lower (upper) Hubbard band.

Received: January 26, 2011
Revised: March 30, 2011
Published: April 22, 2011

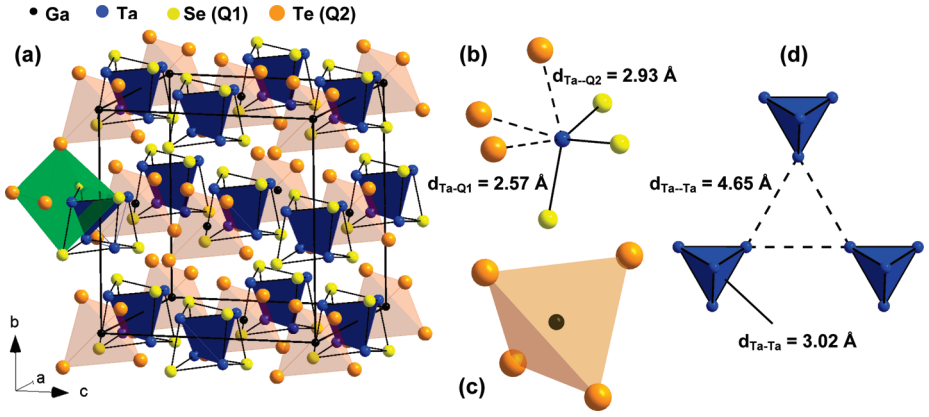

Figure 2. (a) Crystallographic structure of $GaTa_4Se_4Te_4$; (b) octahedral environment of Ta atom with characteristic distances d_{Ta-Q1} and d_{Ta-Q2}; (c) tetrahedral environment of Ga atom; and (d) tetrahedral clusters of Ta atoms with characteristic intercluster d_{Ta-Ta} and intracluster d_{Ta-Ta} distances.

Table 1. Results of the EDS Chemical Analysis Performed on Crystals from Different Batches of $GaTa_4Se_{8-y}Te_y$ (y = 0−6.5)[a]

	atomic % from EDS				
aimed formula	Ga	Ta	Se	Te	formula from EDS [formula from XRD]
y = 1	8.59(90)	29.9(80)	57.59(13)	3.92(10)	$Ga_{1.12(12)}Ta_{3.89(10)}Se_{7.49(2)}Te_{0.51(1)}$ [$GaTa_4Se_{7.51(12)}Te_{0.49(12)}$]
y = 3	8.47(85)	30.69(81)	40.55(15)	20.29(18)	$Ga_{1.10(11)}Ta_{3.99(11)}Se_{5.27(2)}Te_{2.64(2)}$ [$GaTa_4Se_{5.26(10)}Te_{2.74(10)}$]
y = 3.5	8.63(88)	30.02(77)	35.27(13)	26.08(9)	$Ga_{1.12(11)}Ta_{3.90(10)}Se_{4.59(2)}Te_{3.39(1)}$ [$GaTa_4Se_{4.60(6)}Te_{3.40(6)}$]
y = 4	8.65(89)	30.15(77)	30.55(20)	30.65(15)	$Ga_{1.12(12)}Ta_{3.92(10)}Se_{3.97(3)}Te_{3.98(2)}$ [$GaTa_4Se_4Te_4$]
y = 5	8.77(95)	29.80(91)	25.97(13)	35.46(20)	$Ga_{1.14(12)}Ta_{3.87(12)}Se_{3.38(2)}Te_{4.61(3)}$ [$GaTa_4Se_{3.42(13)}Te_{4.58(13)}$]
y = 6	8.54(81)	29.9(72)	15.31(17)	50.1(15)	$Ga_{1.11(11)}Ta_{3.89(10)}Se_{1.99(2)}Te_{6.01(2)}$ [$GaTa_4Se_{2.00(19)}Te_{6.00(19)}$]
y = 7	8.51(87)	29.75(75)	11.64(23)	50.1(11)	$Ga_{1.11(11)}Ta_{3.87(10)}Se_{1.53(3)}Te_{6.51(1)}$ [$GaTa_4Se_{1.47(23)}Te_{6.53(23)}$]

[a] The chemical formulas deduced form the EDS chemical analysis and the XRD refinements are compared.

Interestingly, the AM_4Q_8 Mott insulators exhibit very interesting properties close to the MIT. For example, the substitution of V by Ti in the GaV_4S_8 leads to a filling-controlled MIT and the emergence of a half ferromagnetic metal.[8,9] On the other hand, $GaTa_4Se_8$ and $GaNb_4Se_8$ are rare examples of Mott insulators that undergo a MIT and become superconductors under pressure.[10,11] Last, $GaTa_4Se_8$ exhibits also a striking electric field-induced MIT (also called resistive switching) that may be used in a new concept of nonvolatile memory based on resistance change, called a resistive random access memory (RRAM).[12−16] Various types of MIT were therefore achieved in the narrow gap Mott insulators AM_4Q_8 either by chemical doping, by external pressure, or by electric field. Yet surprisingly a "chemical pressure effect" was never investigated in these systems, while the substitution of the chalcogen atom by a larger one might be an easy way to cause this effect as observed in $NiS_{2-x}Se_x$.

Here, we report the substitution of Se by Te in $GaTa_4Se_8$, and we show that this substitution occurs up to y = 6.5 in $GaTa_4Se_{8-y}Te_y$. Our crystallographic work demonstrates that the substitution takes place first on the chalcogen site around the Ga atoms (site Q2: 16e, $x \approx 0.86$) for $y \leq 4$ and subsequently on the site around the transition metal (site Q1: 16e, $x \approx 0.36$) for a further substitution. Band structure calculations and transport measurements were used to evaluate the effect of the substitution on the electronic properties. This work demonstrates that the Se/Te substitution affects the correlation strength U/W by changing first the bandwidth W up to y = 4 and then the on site repulsion U for $y \geq 4$. This study represents therefore a rare example of U-controlled tuning of the electronic properties in a Mott insulator. Last, this work show that the electric pulse-induced resistive switching phenomenon is observed in the $GaTa_4Se_{8-y}Te_y$ compounds whatever the substitution rate of Se by Te and the correlation strength U/W.

EXPERIMENTAL SECTION

Synthesis. Single crystals of $GaTa_4Se_{8-y}Te_y$ with y ranging from 0 to 6.5 were prepared using stoichiometric mixtures of elemental gallium, tantalum, selenium, and tellurium (purities >99.5%). These mixtures were loaded in evacuated sealed quartz ampules of about 10 cm and heated at 300 °C/h to 1000 °C and hold at this temperature during 160 h. The quartz tubes were subsequently cooled, first slowly to 800 at 1 °C/h and then faster (300 °C/h) to room temperature. These syntheses yielded black powders containing a high yield of $GaTa_4Se_{8-y}Te_y$ metallic-gray cubic and tetrahedral crystals along with a small amount of impurity phases (e.g., GaTe, $TaSe_2$). The maximal crystal sizes vary from one batch to another and range from 30 to 300 μm. All attempts to obtain the pure Te compound $GaTa_4Te_8$ and compounds with y > 6.5 failed.

Chemical Analysis. Semiquantitative chemical analyses were performed with the use of a scanning electron microscope JEOL 5800 equipped with an energy dispersive X-ray (EDX) microanalyzer. For each batch, three crystals were selected, and on average five chemical analyses were performed at different locations of each crystal. Within the same batch, the Te content slightly varies from one crystal to another around the targeted stoichiometry. All results of the chemical analysis are gathered in Table 1.

Table 2. Crystallographic Data, Experimental Details, and Refinement Results for the Structure of Different Compounds $GaTa_4Se_{8-y}Te_y$ (y = 0−6.5)

formula	$GaTa_4Se_8$	$GaTa_4Se_{5.24}Te_{2.76}$	$GaTa_4Se_4Te_4$	$GaTa_4Se_{2.00}Te_{6.00}$	$GaTa_4Se_{1.47}Te_{6.53}$
y(Te)	0	2.76(10)	4.00	6.00(19)	6.53(23)
fw (g/mol)	1425.2	1558.5	1619.8	1717	1742.8
space group			$F\bar{4}3m$		
Z			4		
λ (Å)			0.71069		
a (Å)	10.3746(11)	10.7389(10)	10.8423(11)	10.9955(13)	11.0002(13)
V (Å^3)	1116.6	1238.5	1274.6	1329.4	1331.1
ρ (g/cm^3)	8.4748	8.3558	8.4382	8.5763	8.6939
μ (mm^{-1})	67.445	59.086	56.64	53.132	52.753
θ range (deg)	6.52−34.68	6.58−34.97	6.52−34.85	6.43−34.81	6.43−29.75
no. indep. refl.	223	319	321	331	227
no. variables	11	12	11	12	12
R_{int} (%)	6.09	9.85	8.17	7.52	7.18
R_{obs}/R_{all} (%)	3.68/3.79	2.80/3.09	2.58/2.62	4.75/4.79	4.39/4.45
R_{wobs}/R_{wall} (%)	5.40/5.45	3.83/3.91	3.20/3.22	5.19/5.21	5.97/5.98
residues (e$^-$/Å^3)	1.03/−2.17	1.19/−1.22	1.23/−2.09	2.25/−1.97	2.54/−2.05
			Atomic Positions		
sof (Q1−Se)	1	1	1	0.50(5)	0.37(6)
sof (Q1−Te)	0	0	0	0.50(5)	0.63(6)
sof (Q2−Se)	1	0.31(2)	0	0	0
sof (Q2−Te)	0	0.69(2)	1	1	1
x (Ga)	0	0	0	0	0
x (Ta)	0.60247(5)	0.59937(4)	0.59850(3)	0.59876(8)	0.59878(11)
x (Q1)	0.36537(19)	0.36636(14)	0.36673(10)	0.3632(3)	0.3630(3)
x (Q2)	0.86537(19)	0.86427(10)	0.86367(6)	0.86363(19)	0.8639(3)
			Distances (Å)		
d_{Ta-Ta} (3x)	3.0069(7)	3.0183(6)	3.0207(5)	3.0714(13)	3.0734(17)
$d_{Ta\cdots Ta}$ (3x)	4.3291(7)	4.5753(7)	4.6460(5)	4.7036(13)	4.7049(18)
d_{Ta-Q1} (3x)	2.523(2)	2.5558(16)	2.5689(11)	2.6568(34)	2.6609(35)
d_{Ta-Q2} (3x)	2.768(2)	2.8978(12)	2.9330(7)	2.9705(23)	2.9736(35)
d_{Ga-Q2} (4x)	2.4192(20)	2.5246(11)	2.5602(7)	2.5971(21)	2.5931(33)
D^{TaTa} (%)	44.0(1)	51.6(1)	53.8(1)	53.1(1)	53.1(1)
D^{TaQ} (%)	9.7(2)	13.4(1)	14.2(1)	11.8(2)	11.8(3)

Single-Crystal X-ray Data Collection and Structure Refinement. Single-crystal diffraction experiments were performed using a four circles FR 590 Nonius CAD-4F Kappa-CCD diffractometer at 300 K, using Mo Kα radiation (0.071069 nm wavelength). Numerous crystals with different Te contents were tested for quality (intensity and shape of the spots), and the best crystals were selected for subsequent data collections. All reflection sets for any Te content were consistent with the cubic space group $F\bar{4}3m$. All data treatments, refinement, and Fourier synthesis were carried out with the JANA2006 chain program.[17] Data were corrected for Lorentz and polarization effects, and secondary extinctions correction was applied. The absorption correction was performed using an analytical method taking into account the crystal dimensions by face indexation. For $GaTa_4Se_4Te_4$, as an example, the following set of faces and dimensions were used: (100) 11 μm; (−100) 12 μm; (010) 20 μm; (0−10) 14 μm; (00−1) 22 μm; (001) 23 μm. For $GaTa_4Se_4Te_4$, a set of 314 frames was collected in ω scan mode, with a rotation of 2° and an exposure time of 140 s per frame ; the crystal-to-detector distance was 25 mm. The extinctions and observed reflections were consistent with the cubic space group F-43m. The initial set of 9736 reflections was averaged according to the $m3m$ point group leading to 478 independent reflections (all data) with R_{int} = 0.0817. The structure was refined by considering the atomic coordinates found for $GaTa_4Se_8$. Using these positions, the full-matrix least-squares refinement of the structure converged to R_{obs} = 5.25% for 321 observed reflections ($I > 3\sigma(I)$) and 11 variables. At this stage, the difference Fourier map revealed a negative electron density peak (11 e$^-$/A^3) on the Se site 16e located around the Ga atoms, suggesting the presence of Te on this site. Substituting the Se by Te on this site improved greatly the structure refinement and led to a satisfying reliability factor R_{obs} = 2.58% for 321 observed reflections ($I > 3\sigma(I)$) and 11 variables. We tried to refine a mixed Se/Te occupation on the chalcogen site located around the Ta atoms (site Q1). This mixed site did not improve the refinement, and the Te occupancy did not depart from 0. In the same way, we tried to refine a Ga nonstoichiometry on the occupied site 4a or a partial Ga-occupation of the empty tetrahedral site (4c). This led to a site occupancy that did not depart from 1 or 0, respectively, within the standard deviation. Similar refinements were conducted for all crystals and led to similar results. More details about the data collections, structure refinement, and refined atomic positions are gathered in Table 2 and in Table S1 in the Supporting Information.

X-ray Powder Data Collection. X-ray powder diffraction patterns were recorded at room temperature in the 10−90° 2θ range on a Bruker D8 Advance diffractometer using Cu Kα1 radiation. The PowderCell program[18] was used to simulate the powder pattern using as a structural model the structure refined from the single-crystal study.

dx.doi.org/10.1021/cm200266n |*Chem. Mater.* 2011, 23, 2611–2618

Electrical Measurements. Crystals of $GaTa_4Se_8$, $GaTa_4Se_4Te_4$, $GaTa_4Se_2Te_6$, and $GaTa_4Se_{1.5}Te_{6.5}$ with typical dimensions 300 × 200 × 200 μm^3 were used for electrical transport measurements. Unfortunately, crystal sizes from other batches were not suitable for transport measurements. The selected crystals were contacted with two or four 10 μm gold wires using a carbon paste (Electrodag PR-406) that requires annealing in a vacuum at 150 °C during 30 min. The low-bias resistance was measured using a Keithley 6430 source-measure unit by a standard four-probe technique between 300 and 4.7 K. We checked that the contact resistances were much smaller than the sample resistance at temperatures lower than 150 K. Voltage pulses from 2 to 100 V and from 10 to 50 μs were applied between two probes using an Agilent 8114A pulse generator. During the pulse, the voltage and current across the sample were measured with a Tektronix DPO3034 oscilloscope associated with a IeS-ISSD210 differential probe.

Electronic Band Structure Calculations. Self-consistent electronic structure calculations were performed with the WIEN2k program package using density functional theory (DFT) within the full-potential LAPW method and the Generalized Gradient Approximation (GGA) method. Full-potential LAPW is based on the muffin-tin construction for non overlapping spheres. Within these spheres of radius $R_{mt,\alpha}$ (α = atom type), the angular dependence of the potential $V_\alpha(r)$ is expanded in spherical harmonics $V_\alpha(r) = \Sigma_{lm} V\alpha_{lm}(r) Y^m{}_l(r)$ for $r < R_{mt,\alpha}$. In the intersticial region between the spheres, the potential is represented by a plane wave expansion $V(r) = \Sigma_K V_K e^{iKr}$, with K being the reciprocal lattice vectors. Because of the great flexibility and accuracy of this expansion for the potential and charge density, a very high numerical accuracy is achieved for the LAPW method. Mixed LAPW and APW + lo (lo = local orbitals) basis sets were used to increase the efficiency of the APW linearization. Further technical details can be found in ref 19.

The total energies and charge densities of the SCF cycles converged to changes respectively smaller than 1×10^{-4} Ry cell^{-1} and 1×10^{-3} electron cell^{-1}. The basis sets consisted of plane waves up to a cutoff $R_{mt}K_{max} = 9.00$. The atomic sphere radii R_{mt} and k-points mesh used in the irreducible wedges of the Brillouin zone for each structure are shown in Table S2 in the Supporting Information. Calculations were performed using the refined structures for $GaTa_4Se_8$, $GaTa_4Se_4Te_4$, and $GaTa_4Se_2Te_6$. Unfortunately, we were not able to perform band structure calculations for the other refined structures, because the necessary unit cell dimensions required to account for mixed Se/Te sites are much too large for such calculations. To keep the size of the unit cell reasonable, we have therefore computed the band structures of compounds with mixed sites only for $GaTa_4Se_6Te_2$ and $GaTa_4Se_2Te_6$. As $GaTa_4Se_6Te_2$ was not synthesized during this work, the structure used to compute the band structure of $GaTa_4Se_6Te_2$ was obtained by interpolation of the atomic positions and unit cell parameters between the closest structures refined during our crystallographic study (i.e., $GaTa_4Se_{7.5}Te_{0.5}$ and $GaTa_4Se_{5.3}Te_{2.7}$). Moreover, the symmetry of both structures of $GaTa_4Se_6Te_2$ and $GaTa_4Se_2Te_6$ was lowered from $F\bar{4}3m$ to $C222_1$ (No. 20) to reproduce the mixed Se/Te site. Finally, we have also performed a band structure calculation for the unstable $GaTa_4Te_8$ compound using an extrapolated structure ($F\bar{4}3m$). The crystallographic structures used to compute the band structures of $GaTa_4Se_6Te_2$, $GaTa_4Se_2Te_6$, and $GaTa_4Te_8$ are described in Tables S3, S4, and S5 in the Supporting Information.

RESULTS AND DISCUSSION

External pressure is a classical way to modulate the bandwidth (W) and so to tune the correlation strength (U/W) in a Mott insulator. In NiS_2, external pressure induces an increase of W so huge that it results in the breakdown of the Mott insulating state (i.e., a bandwidth-controlled MIT).[1,2] In this system, the partial substitution of S atoms by larger Se atoms is generally believed to lead to an effect similar to external pressure.[1,2] This effect is usually referenced as a "chemical pressure effect". To induce a similar "chemical pressure effect" in the Mott insulator $GaTa_4Se_8$, we substituted the Se atoms by the larger Te atoms (see Experimental Section). For $y \leq 6.5$, these syntheses yielded black powder samples whose X-ray powder patterns were similar to that of the nonsubstituted compound $GaTa_4Se_8$. Figure 3 shows, for example, the powder pattern recorded for $GaTa_4Se_4Te_4$, which evidences the good purity of this sample. All of these products contained also tetrahedral or cubic crystals with edge length in the 30−300 μm range. For all batches, several crystals were selected and analyzed by EDX. Chemical analyses revealed a composition containing all four elements Ga, Ta, Se, and Te (see Figure S1 in the Supporting Information) with a ratio in good agreement with the targeted chemical formulation $GaTa_4Se_{8-y}Te_y$ ($y < 6.5$) (see Table 1). For synthesis performed with larger Te content ($y > 6.5$), no crystals were obtained, and a powder X-ray

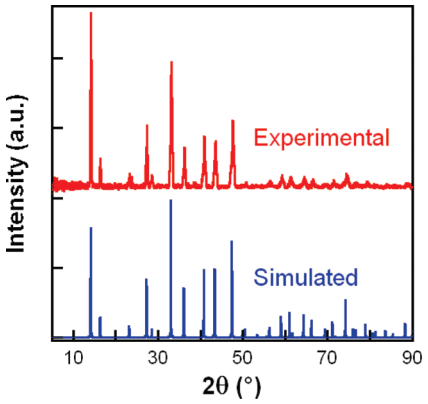

Figure 3. X-ray powder diffraction pattern of $GaTa_4Se_4Te_4$ (top curve). This experimental powder pattern agrees well with the pattern simulated using the structure as solved from the single-crystal study (bottom curve).

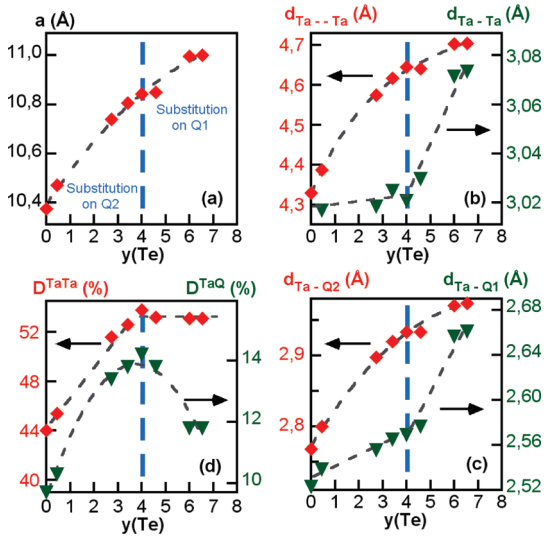

Figure 4. Evolution versus Te content y in $GaTa_4Se_{8-y}Te$ of the (a) unit cell parameter (b) Ta--Ta long intercluster and Ta—Ta short intracluster distances, (c) Ta—Q2 and Ta—Q1 interatomic distances, and (d) degree of clustering D^{TaTa}, defined as $(d_{M---M}/d_{M-M}) - 1$, and of the degree of distortion D^{TaQ}, defined as $(d_{M-Q2}/d_{M-Q1}) - 1$. The blue dashed line shares the two different substitution areas: Te on Q2 special position for the left part and on Q1 special position for the right part.

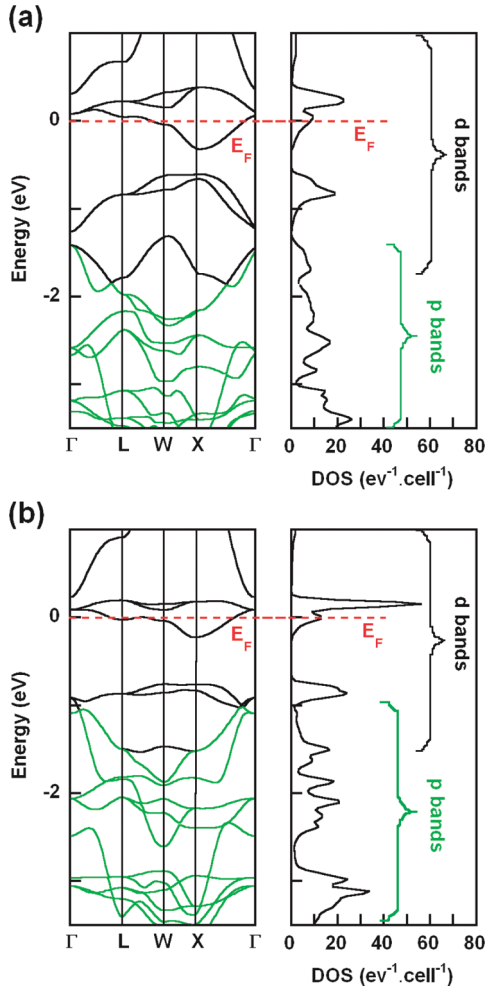

Figure 5. Band structures (left panels) and DOS (right panels) calculated for (a) $GaTa_4Se_8$ and (b) $GaTa_4Se_4Te_4$, with $\Gamma(0,0,0)$, $L(1/2,1/2,1/2)$, $W(1/2,0,1)$, and $X(0,0,1)$ in the conventional Brillouin zone of $F\bar{4}3m$.

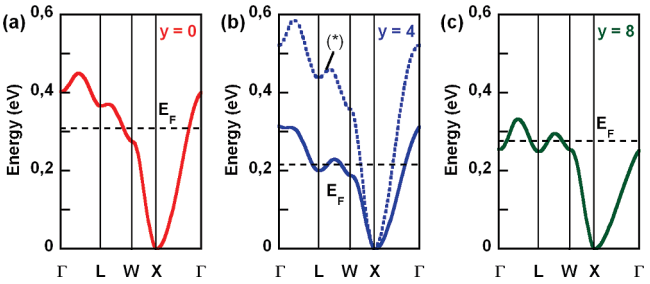

Figure 6. Comparison of the bandwidth of the Ta d band crossing the Fermi level for (a) $GaTa_4Se_8$, (b) $GaTa_4Se_4Te_4$ (solid line), and (c) hypothetical $GaTa_4Te_8$ compounds. The dashed line (*) in panel (b) corresponds to the band dispersion calculated for an hypothetical structure of $GaTa_4Se_4Te_4$, imagined using the cell parameter and atomic positions of $GaTa_4Se_8$ but replacing Se by Te on site Q2. The horizontal straight dashed line represents the Fermi energy.

diffraction analysis of the synthesized products revealed a mixture of binary compounds, mainly $GaTe_x$ and $TaSe_2$.

The structures of all compounds $GaTa_4Se_{8-y}Te_y$ ($y < 6.5$) were refined by means of X-ray diffraction as described in the Experimental Section (see Table 2 and Table S1 in the Supporting Information for more details). The refinement revealed that all of these compounds adopt a deficient spinel type structure (space group $F\bar{4}3m$ from $y = 0$ to $y = 6.5$). Figure 4 displays the evolution of the cell parameter along the series. A monotonous increase of the cubic cell parameter (reminding a Veggard law) is observed when increasing the Te content. This is already a strong sign of the partial substitution of Se by Te. Structure refinement of all $GaTa_4Se_{8-y}Te_y$ ($y < 6.5$) compounds confirmed the partial substitution of Se by Te and led to refined chemical formula in good agreement with the analyzed one (see Table 1). However, a first issue with this substitution concerns the location of the Te atoms. The $GaTa_4Q_8$ compounds consist of Ta_4 clusters embedded in heterocubane-like $[Ta_4Q_4]^{5-}$ entities and $[GaQ_4]^{5+}$ tetrahedra arranged in a NaCl-like manner (see Figure 2a). Therefore, two chalcogen sites exist in this structure, one within the cubanes Ta_4Q_4 entities (site Q1: 16e, $x \approx 0.36$) and another one around the Ga atoms (site Q2: 16e, $x \approx 0.86$). Interestingly, our crystallographic work (see Table 2) clearly demonstrates that the Se/Te substitution in $GaTa_4Se_{8-y}Te_y$ arises first (for $0 \le y \le 4$) within the GaQ_4 tetrahedra and subsequently ($4 < y < 6.5$) within the Ta_4Q_4 cubanes. The structure of $GaTa_4Se_4Te_4$, shown in Figure 2, is therefore of special interest because it is built up as a simple arrangement of pure Ta_4Se_4 and $GaTe_4$ entities, according to structure refinement results. The analysis of the main interatomic distances (see Table 2, Table S1, and Figure 4) reveals striking changes of behaviors at the composition $y = 4$ within the solid solution. In the $0 \le y \le 4$ range, the Se/Te substitution within the GaX_4 tetrahedra (Q2 site) barely affects the Ta_4 tetrahedral cluster (d_{Ta-Ta} increases from 3.007 to 3.025 Å) but strongly increases the separation between these clusters ($d_{Ta\cdots Ta}$ increases from 4.33 to 4.65 Å). These trends are completely reversed for $4 < y \le 6.5$ because the substitution within the Ta_4X_4 cubane entities increases the intracluster distances Ta (d_{Ta-Ta} raises to 3.073 Å) but scarcely affects the separation between these clusters ($d_{Ta\cdots Ta}$ stays around 4.7 Å). Interestingly, the parameters used in ref 11 to describe the distortion of the lacunar spinel AM_4Q_8 with respect to the ideal AM_2Q_4 spinel structure also display inflection points at $y = 4$ (Figure 4d). From this simple analysis of the structural data, we may therefore expect that the substitution induces very different effects on the electronic properties of $GaTa_4Se_{8-y}Te_y$ depending on whether the substitution occurs on the Q2 ($0 \le y \le 4$) or on the Q1 ($4 < y \le 6.5$) sites.

To quantify the effect of the chalcogen substitution on the electronic structure, we performed band structure calculations for $GaTa_4Se_8$, $GaTa_4Se_6Te_2$, $GaTa_4Se_4Te_4$, $GaTa_4Se_2Te_6$, as well as for hypothetical compound $GaTa_4Te_8$ (see Figures 5, 6, and S3; details are given in the Experimental Section). Unfortunately, the LDA+U technique that takes into account the electronic correlation (U) is not appropriate to compute the band structures of the $GaTa_4Se_{8-y}Te_y$ compounds, because these compounds are degenerated Mott insulators. The band crossing the Fermi level is indeed 3-fold degenerated at the Γ point, which makes impossible the use of the LDA+U technique as implemented in the frame of the WIEN2k code. The GGA approximation was therefore employed, which of course does not allow one to handle properly the correlation effect expected in these Mott insulators. Despite this bad description of correlation effects, which entails erroneous metallic ground states for all compounds (see Figures 5 and 6), GGA calculations still reveal key features of $GaTa_4Se_{8-y}Te_y$ band structures. First, they show that the electronic structure of these

dx.doi.org/10.1021/cm200266n |Chem. Mater. 2011, 23, 2611–2618

Table 3. Values of the Calculated Bandwidth (W), the Measured Activation Energy (E_A), and the Estimated Electronic Correlation Energy (U) for Different $GaTa_4Se_{8-y}Te_y$ (y = 0−6.5) Compounds

compound	$GaTa_4Se_8$	$GaTa_4Se_6Te_2$	$GaTa_4Se_4Te_4$	$GaTa_4Se_2Te_6$	$GaTa_4Se_{1.5}Te_{6.5}$	$GaTa_4Te_8$[a]
bandwidth W (meV)	450	352	314	332	332[b]	333
E_A (meV)	241		293	171	115	
$E_A + W$ (~U) (meV)	691		607	503	447	

[a] Unknown compound. [b] Estimated value from the $W = f(y)$ curve in Figure 7.

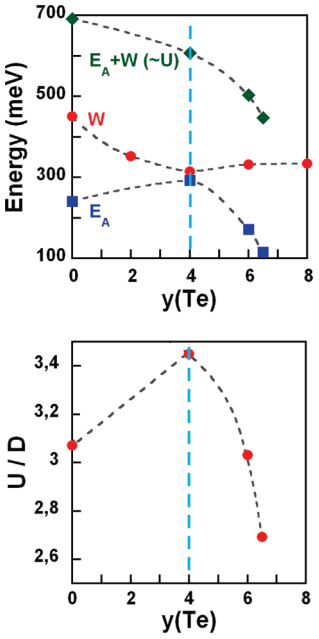

Figure 7. (a) Evolution of the bandwidth W, the activation energy E_A, and the estimated correlation energy U (=W+E_A) as a function of the Te content y in $GaTa_4Se_{8-y}Te_y$. (b) Evolution of the correlation strength U/D (=$2U/W$) within the $GaTa_4Se_{8-y}Te_y$ series. Lines are a guide for the eyes.

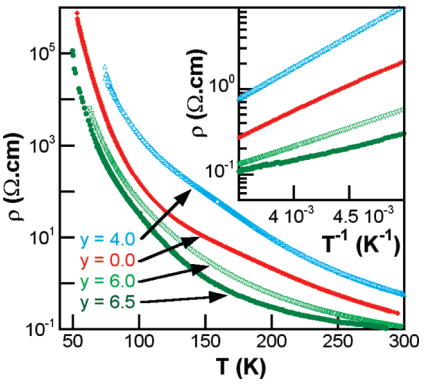

Figure 8. Temperature dependence of the resistivity for different compounds $GaTa_4Se_{8-y}Te_y$ (y = 0, 4, 6, 6.5). Inset resitivity versus $1/T$: the straight line observed in this representation indicates an activation law.

compounds is rather simple, with weakly hybridized Ta 5d bands at the Fermi level clearly separated from the chalcogen p bands located at lower energy. Even the Te 5p states, expectedly located at higher energy than the Se 4p states, do not play any crucial role at the Fermi level. As a consequence, the $GaTa_4Q_8$ compounds can be considered as prototypical Mott insulators following the Zaanen−Sawatsky−Allen (ZSA) classification,[20] that is, with a Mott−Hubbard gap between correlated purely d-states (see Figure 1). On the other hand, the GGA calculations give access to the bandwidth of the three degenerated bands near the Fermi level, and this analysis allows discussing the relative variations of the bandwidth within the series of $GaTa_4Se_{8-y}Te_y$ compounds (see Figure 5). Figure 6 displays the band dispersion of the Ta 5d band crossing the Fermi level for different $GaTa_4Se_{8-y}Te_y$ compounds. In Table 3 are listed the calculated bandwidths for all compounds. In Figure 7a is plotted the bandwidth (W) versus Te content. First, we observe a narrowing of the band crossing the Fermi level from $GaTa_4Se_8$ (450 meV) to $GaTa_4Se_4Te_4$ (314 meV), and the bandwidth stays almost constant for larger Te contents (i.e., 330 meV for $GaTa_4Se_2Te_6$ and $GaTa_4Te_8$). The band narrowing in the $0 \le y \le 4$ range is quite surprising. We were rather expecting a band broadening according to a "chemical pressure effect". To understand this discrepancy, we have performed another calculation for a hypothetical $GaTa_4Se_4Te_4$ structure using the atomic positions and cell parameter of the real $GaTa_4Se_8$ compound, but replacing on the Q2 site the Se^{2-} ion (ionic radius 198 pm) by the larger Te^{2-} ion (221 pm). According to this calculation, the band narrowing in the $0 \le y \le 4$ range can be rationalized as follows. The bandwidth of the Ta 5d bands crossing the Fermi level is mainly driven by the dispersion along the Γ−X direction, that is, from the [100], [010], and [001] directions in real space. Comparison of our calculations with different chalcogen on the Q2 site (see Figure 6a,b) demonstrates that the transfer integral between two Ta_4 clusters along the Γ−X direction is mediated by the chalcogen on the Q2 site and does not correspond to a direct Ta−Ta bond. The bandwidth of $GaTa_4Se_8$, 450 meV (see Figure 6a), indeed increases to 580 meV (see Figure 6b) by replacing Se by the larger atom Te on the Q2 site. The bandwidth narrowing observed between $GaTa_4Se_8$ (450 meV) and the real $GaTa_4Se_4Te_4$ compound (314 meV) therefore implies that the increase of the Ta−Q2 distance (see Figure 4c) overcompensates the increase of the chalcogen size and subsequently lowers the tantalum−chalcogen orbital mixing. As a conclusion, all of these calculations reveal that the Se/Te substitution induces a negative "chemical pressure effect" for $0 \le y \le 4$ in $GaTa_4Se_{8-y}Te_y$ and suggest that the correlation strength U/W and the Mott Hubbard gap should increase in the corresponding substitution range.

Resistivity measurements are likely one of the easiest way to check for such variations of the Mott−Hubbard gap. Four-probe resistivity measurements were therefore performed on the following members of the $GaTa_4Se_{8-y}Te_y$ solid solution: $GaTa_4Se_8$, $GaTa_4Se_4Te_4$, $GaTa_4Se_2Te_6$, and $GaTa_4Se_{1.5}Te_{6.5}$. Unfortunately, as mentioned in the Experimental Section, crystals for other compositions were too small to enable four probe measurements. Figure 8 displays the resistivity of the different compounds. At first glance, this figure reveals that all compounds exhibit a semiconducting behavior and therefore that the MIT was not reached through the

dx.doi.org/10.1021/cm200266n |Chem. Mater. 2011, 23, 2611–2618

substitution of the chalcogen atom. Above 200 K, the resistivity follows a classical activation energy law $\rho = \rho_0 e^{E_A/2kT}$, where E_A is the activation energy. Table 3 summarizes the activation energy for all crystals, and Figure 7a shows a plot of E_A versus Te content. It appears that E_A increases from $y = 0$ to $y = 4$ (i.e., when substituting the chalcogen atom on the site Q2), and then decreases for larger Te content $y > 4$ (i.e., when substituting the chalcogen atom on the site Q1).

To get more insight on the effect of the substitution of the chalcogen atoms on the electronic structure of $GaTa_4Se_{8-y}Te_y$, we now compare the results of our calculations with our structural and resistivity data. First, we note that the evolution of E_A versus Te content could not be expected on the sole analysis of the bandwidth evolution through the series (see Figure 7). More interestingly, Figure 7 also displays the sum of E_A and W as a function of y. As would confirm a simple observation of Figure 1, $E_A + W$ is in a first approximation a crude estimation of the correlation energy U in these compounds if we assume E_A to be close to the Mott−Hubbard gap. This assumption is supported by recent measurement of optical conductivity data for $GaTa_4Se_8$, which provides a band gap value in good agreement with the activation energy measured for this compound.[21] Interestingly, Figure 7 shows that $E_A + W$ decreases only slightly for a Te content ranging from $y = 0$ to 4 (Se/Te substitution on the Q2 site), and then decreases much more for larger Te content $y > 4$ (Se/Te substitution on the Q1 site). This analysis strongly suggests that the Te addition on site Q2 (for $0 \le y \le 4$) has only a small influence on the electronic correlation on the Ta clusters, while the Te addition on site Q1 strongly decreases the on-site electronic repulsions (U) on the Ta clusters. To understand this behavior, reexamination of Figure 4, which displays the evolution of the intracluster distances d_{Ta-Ta} along the series of compound $GaTa_4Se_{8-y}Te_y$, is of great interest. Indeed, this figure shows clearly that the clusters expansion is much weaker when the substitution occurs on site Q2 (for $0 \le y \le 4$) than when the Te addition occurs on site Q1 (for $4 < y \le 6.5$). As in the $GaTa_4Se_{8-y}Te_y$ Mott insulators the electronic correlation occurs on the cluster molecular orbital, a strong expansion of these clusters may easily account for the decrease observed for the electronic correlation (U).

From all of these experimental and theoretical results, a clear picture emerges about the effect of the substitution of the chalcogen atoms in the $GaTa_4Se_{8-y}Te_y$ Mott insulators. The substitution on special position Q2, that is, on going from $GaTa_4Se_8$ to $GaTa_4Se_4Te_4$, increases the separation between barely affected Ta clusters, which results in a strong decrease of the bandwidth (W) while the electronic correlation (U) stays almost constant. As a consequence, it leads to an increase of the correlation strength and therefore of the Mott Hubbard gap. This evolution appears clearly in Figure 7b, which depicts the evolution of the correlation strength in the series of $GaTa_4Se_{8-y}Te_y$ compounds (this figure uses the convention of the dynamical mean-field theory (DMFT), and U/D is plotted instead of U/W, where $D = W/2$ represents one-half of the bandwidth). On the other hand, the chalcogen substitution on site Q1 (for $4 < y \le 6.5$) increases the cluster's size, which results in a strong decrease of the correlation U on the clusters. Meanwhile, the separation between these clusters is barely affected, which leaves the bandwidth almost unchanged. As a consequence, for $y > 4$ the correlation strength U/D and therefore the Mott Hubbard gap decrease (see Figure 7).

This analysis highlights therefore that the substitution of the chalcogen atoms and physical pressure do not have equivalent effects in the $GaTa_4Se_{8-y}Te_y$ Mott insulators in contrast to other chalcogenide systems such as $NiS_{2-x}Se_x$. Indeed, as reported for $GaTa_4Se_8$ in ref 11, under physical pressure the Ta−Ta distance within the cluster stays almost constant but the Ta--Ta distance between the cluster is strongly reduced. As a consequence, we expect that U stays almost constant and the bandwidth W increases. This is a typical W-controlled scenario as depicted in textbook, which leads to a strong lowering of the Mott−Hubbard gap and ultimately to a MIT. Contrary to external pressure, the substitution of the chalcogen atoms in $GaTa_4Se_{8-y}Te_y$ does not lead to a W-controlled scenario. Instead, we observe first an inverse W-controlled scenario leading to a gap increase (and of U/W for $0 \le y \le 4$) and second a U-controlled scenario leading to a decrease of the gap (and of U/W for $4 < y \le 6.5$). Even though the Se/Te substitution does not lead to a MIT, we note that the value of $U/D \approx 2.7$ reached for the most substituted compound $GaTa_4Se_{1.5}Te_{6.5}$ (see Figure 7) is extremely close to the critical values $(U/D)_c \approx 2.5 \pm 0.5$ below which an insulator to metal transition is predicted by modern theories describing Mott insulators.[22] This demonstrates that the Se/Te substitution above $y = 4$ in $GaTa_4Se_{8-y}Te_y$ drives these compounds very near to a U-controlled Mott transition. This is quite remarkable, as in all known Mott insulators, the modification of the correlation strength U/W was achieved only by changing the bandwidth W. Although theoretically possible, a tuning of the correlation strength U/W by a modification of the U value was, to our knowledge, never realized experimentally so far. The electronic repulsion U is indeed a quantity specific to each transition metal, which, contrary to the bandwidth, can hardly be changed continuously. Conversely, a tuning of U is possible in the AM_4Q_8 compounds because the correlated units are the Ta_4 clusters whose size may be modified by the Te substitution ($y > 4$). In that respect, the $GaTa_4Se_{8-y}Te_y$ compounds may be the first Mott insulator series where a U-controlled tuning of electronic properties is possible.

We now turn our attention on the consequences of this peculiar substitution of Se by Te on the resistive switching in the $GaTa_4Se_{8-y}Te_y$ compounds. As was already mentioned, the nonsubstituted $GaTa_4Se_8$ compound exhibits a striking electric field-induced nonvolatile resistive switching that may be of interest to build a new class of nonvolatile memory RRAM.[12−16] We found that this nonvolatile resistive switching is concomitant to the formation of an electronic phase separation. Moreover, this nonvolatile resistive switching leads to a granular superconducting state closely related to the bulk superconductivity induced by pressure in $GaTa_4Se_8$. This fingerprint of a pressure-induced insulator−metal−superconductor transition suggests that the nonvolatile RS is somewhat related to a bandwidth-controlled Mott transition. In that respect, the substitution of Se by Te may affect or even suppress the nonvolatile resistive switching as it induces a negative chemical pressure effect in the $GaTa_4Se_{8-y}Te_y$ compounds. We have therefore studied the resistive switching in the substituted compounds $GaTa_4Se_{8-y}Te_y$. Voltage pulses were applied at 77 K on crystals of $GaTa_4Se_4Te_4$, $GaTa_4Se_2Te_6$, and $GaTa_4Se_{1.5}Te_{6.5}$, as described in the Experimental Section. Figure 9 shows the temperature dependence of the resistivity before and after a 10 μs pulse of 99 V (20 kV/cm) in $GaTa_4Se_4Te_4$. A clear nonvolatile RS is observed for this crystal with a lowering of the resistance of more than 1 order of magnitude at 77 K. Similar nonvolatile RS are also shown in Figure 9 for $GaTa_4Se_2Te_6$ (with a pulse of 12 kV/cm) and $GaTa_4Se_{1.5}Te_{6.5}$ (with a pulse of 12 kV/cm). Moreover, we found that $GaTa_4Se_4Te_4$ crystals can switch back and forth between their high and low

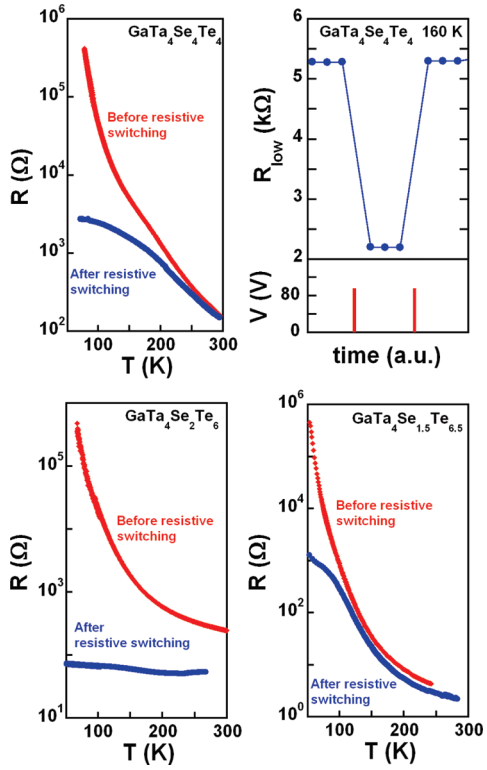

Figure 9. Temperature dependence of the resistance before and after the application of electric pulses inducing a nonvolatile resistive switching in different compounds $GaTa_4Se_{8-y}Te_y$ (y = 4, 6, 6.5). The upper right panel shows a cycling between two different resistance states obtained for $GaTa_4Se_4Te_4$ at 160 K thanks to two successive 10 μs 100 V pulses.

resistance states by application of successive electric pulses at 160 K (Figure 9). All of these results demonstrate therefore that the substitution of Se by Te does not totally suppress the nonvolatile resistive switching. However, we note that the nonvolatile RS seems to be reached with a lower electric field for compounds having lower correlation strengths. Yet this trend cannot be fully ascertained at this step of our work and further studies are needed to address thoroughly this point.

CONCLUSIONS

We have explored the substitution of Se by Te in the lacunar spinel compound $GaTa_4Se_8$. Our synthesis work shows that the pure Te compound does not exist and that the solid solution $GaTa_4Se_{8-y}Te_y$ reaches a limit for y = 6.5. Our crystallographic work demonstrates that Te atoms substitute first the chalcogen site around the Ga atoms (site Q2: 16e, $x \approx 0.86$) for $y \leq 4$ and subsequently the chalcogen site around the transition metal (site Q1: 16e, $x \approx 0.36$). Band structure calculations show that the substitution of Se by Te around the Ga site, that is, on going from $GaTa_4Se_8$ to $GaTa_4Se_4Te_4$, decreases the bandwidth W. Resistivity measurements reveal that the Mott Hubbard gap increases, which confirms that the correlation strength U/W increases also. On the other hand, the chalcogen substitution around the Ta atoms (site Q1) does not affect the bandwidth (W) but decreases the Mott Hubbard gap and the correlation strength U/W through a strong lowering of the correlation (U) on the clusters. All of our results demonstrate therefore that the substitution of Se by the larger Te atom in $GaTa_4Se_{8-y}Te_y$ does not lead to a classical and expected chemical pressure effect that would result in a simple increase of the bandwidth as observed in the other chalcogenide Mott insulator system $NiS_{2-x}Se_x$. Finally, our work shows that the substitution of Se by Te in $GaTa_4Se_{8-y}Te_y$ does not suppress the electric pulse-induced resistive switching phenomena observed in the nonsubstituted compound $GaTa_4Se_8$ even though this substitution introduces some disorder and some changes in the correlation strength U/W.

ASSOCIATED CONTENT

Supporting Information. Additional tables and figures (PDF). Crystallographic information (CIF). This material is available free of charge via the Internet at http://pubs.acs.org.

AUTHOR INFORMATION

Corresponding Author

*E-mail: laurent.cario@cnrs-imn.fr.

REFERENCES

(1) Imada, M.; Fujimori, A.; Tokura, Y. *Rev. Mod. Phys.* **1998**, *70*, 1039.
(2) Honig, J. M.; Spalek, J. *Chem. Mater.* **1998**, *10*, 2910–2929.
(3) McWhan, D. B.; Remeika, J. P. *Phys. Rev. B* **1970**, *2*, 3734–3750.
(4) Lupi, S.; Baldassarre, L.; Mansart, B.; Perucchi, A.; Barinov, A.; Dudin, P.; Papalazarou, E.; Rodolakis, F.; Rueff, J.-P.; Itié, J.-P.; Ravy, S.; Nicoletti, D.; Postorino, P.; Hansmann, P.; Parragh, N.; Toschi, A.; Saha-Dasgupta, T.; Andersen, O. K.; Sangiovanni, G.; Held, K.; Marsi, M. *Nat. Commun.* **2010**, *1*, 105.
(5) Yao, X.; Honig, J. M.; Hogan, T.; Kannewurf, C.; Spalek, J. *Phys. Rev. B* **1996**, *54*, 17469–17475.
(6) Ben Yaich, H.; Jegaden, J. C.; Potel, M.; Sergent, M.; Rastogi, A. K.; Tournier, R. *J. Less-Common Met.* **1984**, *102*, 9.
(7) Johrendt, D. *Z. Anorg. Allg. Chem.* **1998**, *624*, 952–958.
(8) Dorolti, E.; Cario, L.; Corraze, B.; Janod, E.; Vaju, C.; Koo, H. J.; Kan, E.; Whangbo, M. H. *J. Am. Chem. Soc.* **2010**, *132*, 5704–5710.
(9) Vaju, C.; Martial, J.; Janod, E.; Corraze, B.; Fernandez, V.; Cario, L. *Chem. Mater.* **2008**, *20*, 2382–2387.
(10) Abd-Elmeguid, M. M.; Ni, B.; Khomskii, D. I.; Pocha, R.; Johrendt, D.; Wang, X.; Syassen, K. *Phys. Rev. Lett.* **2004**, *93*, 126403.
(11) Pocha, R.; Johrendt, D.; Ni, B. F.; Abd-Elmeguid, M. M. *J. Am. Chem. Soc.* **2005**, *127*, 8732–8740.
(12) Cario, L.; Vaju, C.; Corraze, B.; Guiot, V.; Janod, E. *Adv. Mater.* **2010**, *22*, 5193–5197.
(13) Dubost, V.; Cren, T.; Vaju, C.; Cario, L.; Corraze, B.; Janod, E.; Debontridder, F.; Roditchev, D. *Adv. Funct. Mater.* **2009**, *19*, 2800–2804.
(14) Souchier, E.; Cario, L.; Corraze, B.; Moreau, P.; Mazoyer, P.; Estounès, C.; Retoux, R.; Janod, E.; Besland, M.-P. *Phys. Status Solidi RRL* **2011**, *5*, 53–55.
(15) Vaju, C.; Cario, L.; Corraze, B.; Janod, E.; Dubost, V.; Cren, T.; Roditchev, D.; Braithwaite, D.; Chauvet, O. *Adv. Mater.* **2008**, *20*, 2760.
(16) Vaju, C.; Cario, L.; Corraze, B.; Janod, E.; Dubost, V.; Cren, T.; Roditchev, D.; Braithwaite, D.; Chauvet, O. *Microelectron. Eng.* **2008**, *85*, 2430.
(17) Petricek, V.; Dusek, M.; Palatinus, L. *JANA 2006*; Academy of Science of Cseck Republic: Praha, 2006.
(18) Kraus, W.; Nolze, G. *PowderCell for Windows*, 2.4 ed.; 2000.
(19) Blaha, P.; Schwarz, K.; Madsen, G.; Kvasnicka, D.; Luitz, J. *WIEN2K*; 2001.
(20) Zaanen, J.; Sawatzky, G. A.; Allen, J. W. *Phys. Rev. Lett.* **1985**, *55*, 418.
(21) Taphuoc, V., to be published.
(22) Georges, A.; Kotliar, G.; Krauth, W.; Rozenberg, M. J. *Rev. Mod. Phys.* **1996**, *68*, 13.